frontiers | Frontiers in Earth Science

TYPE Original Research
PUBLISHED 12 April 2023
DOI 10.3389/feart.2023.1177629

OPEN ACCESS

EDITED BY
Xingqi Liu,
Capital Normal University, China

REVIEWED BY
Xujiao Zhang,
China University of Geosciences, China
Xi Chun,
Inner Mongolia Normal University, China

*CORRESPONDENCE
LuPeng Yu,
yulupeng319@126.com

†These authors have contributed equally to this work

SPECIALTY SECTION
This article was submitted to Quaternary Science, Geomorphology and Paleoenvironment, a section of the journal Frontiers in Earth Science

RECEIVED 01 March 2023
ACCEPTED 27 March 2023
PUBLISHED 12 April 2023

CITATION
Liu J, Fan H, An P, Wen H and Yu L (2023), Mega-lake formation in the eastern Hetao Basin, China, during marine isotope stages 7 and 5: A comparison of quartz and feldspar luminescence dating. *Front. Earth Sci.* 11:1177629. doi: 10.3389/feart.2023.1177629

Mega-lake formation in the eastern Hetao Basin, China, during marine isotope stages 7 and 5: A comparison of quartz and feldspar luminescence dating

JianGang Liu[1,2†], HaiYan Fan[1,2†], Ping An[2], Huan Wen[1,2] and LuPeng Yu[2*]

[1]School of Geography, Liaoning Normal University, Dalian, China, [2]Luminescence Research Laboratory, Shandong Provincial Key Laboratory of Water and Soil Conservation and Environmental Protection, School of Resource and Environmental Sciences, Linyi University, Linyi, China

Paleo-lacustrine sediments indicate that a mega-lake developed in the Hetao Basin (HTB), suggesting dramatic changes in the geomorphology and surface process of the Yellow River and surrounding regions. However, the formation time of the mega Hetao paleo-lake (HTPL) in the HTB remains unclear. In this study, a set of 7.6-m-thick lacustrine sediments in the middle of the HTB is dated by both quartz optically stimulated luminescence (OSL) and K-feldspar (KF) post-infrared infrared stimulated luminescence (p-IR IRSL, pIRIR). The results are as follows. 1) The quartz OSL ages do not increase with depth as the KF pIRIR ages displayed but are saturated at ca. 80–100 ka with the consequence of age underestimation. The influence of signal saturation may occur below 96 Gy (ca. 32 ka) in this region. Thus, the KF pIRIR ages are chosen for geomorphological evolution reconstruction. 2) These ages suggest the level of the HTPL exceeded 1033 m asl twice—at the early stages of MIS 7 (~255–245 ka) and MIS 5 (~130–120 ka). However, the exact scale of the HTPL and its relationship with the Jilantai paleo-lake is unclear. 3) This chronology suggests strong linkage between periodic formation of the HTPL and glacial-scale climatic change. We therefore propose an alternative hypothesis to interpret these processes: the Hobq dunefield expanded eastward to dam the narrow Jin-Shaan Gorge during the glacial periods when the flow of the Yellow River was weak. Then, in the beginning of the interglacial periods, the basin was filled by abruptly resumed runoff in response to increased glacial meltwater and precipitation on the northeastern Tibetan Plateau. Once the lake spilt out, the loose dune dam was quickly breached.

KEYWORDS

Hobq Dunefield, Hetao paleo-lake, aeolian–fluvial interactions, dune damming, Yellow River, OSL and pIRIR dating

1 Introduction

Lacustrine sediments are important paleoclimatic archives due to their continuity, sensitivity, and high resolution (Wang et al., 2009; Shen, 2012), especially in the arid and semi-arid regions of the Tibetan Plateau (TP) where continuous terrestrial sedimentary records are difficult to preserve (Yu et al., 2022). At the boundary of the modern East Asian Summer Monsoon (EASM), a mega Hetao paleo-lake (HTPL) has been reconstructed based

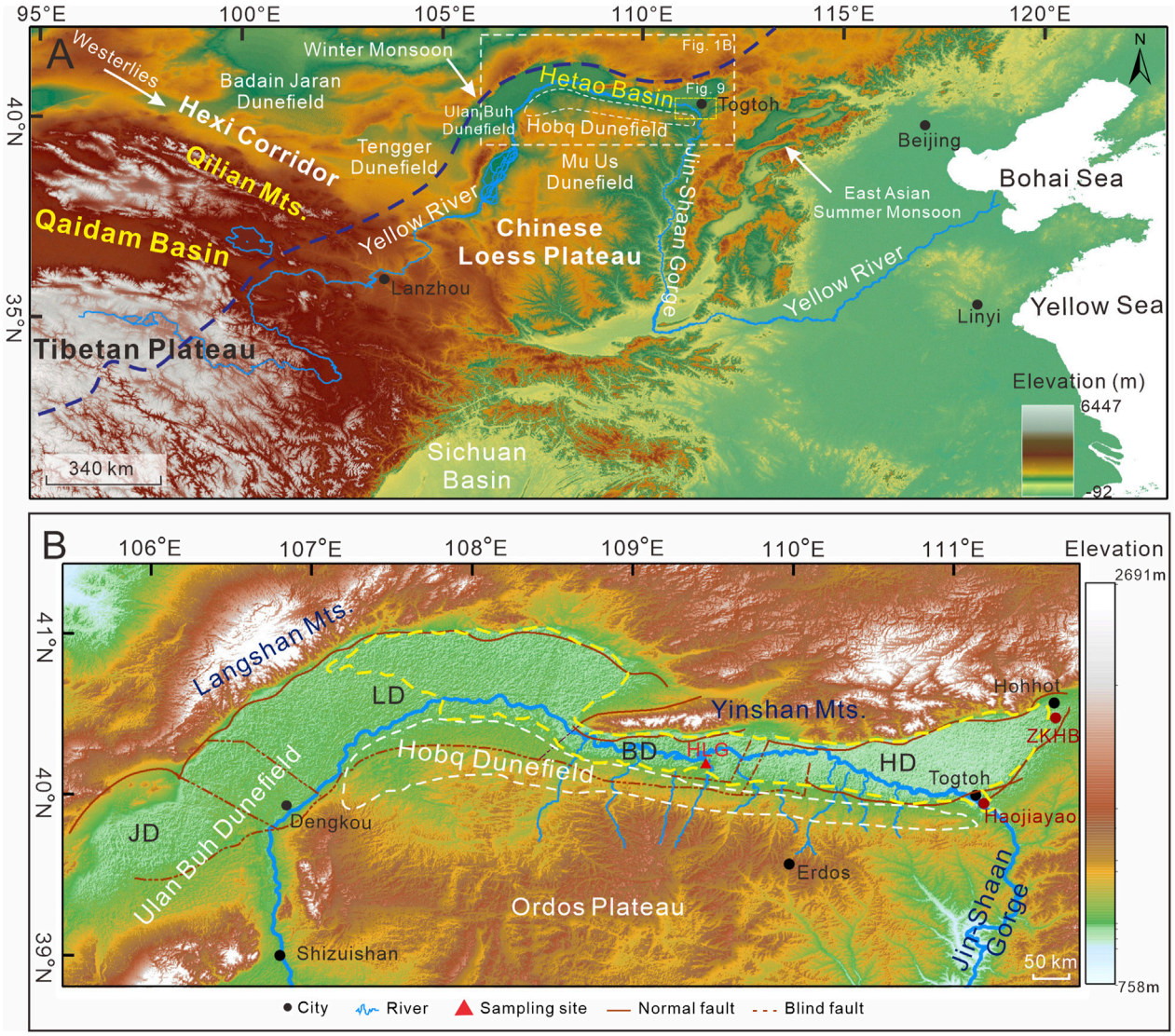

FIGURE 1
Geographic setting of the Hetao Basin. **(A)** Location of study area, major atmospheric circulation systems, and boundary of the EASM (dotted blue line). **(B)** DEM shows morphology of regions around the Hetao Basin, including modern drainage system of the Yellow River, and the faults (red lines) (modified from CEA, 1988) dividing the basin into four sub-basins: Jilantai (JD), Linhe (LD), Baiyanhua (BD), and Hohhot Depressions (HD). The location of ZKHB and Haojiayao cores (red dots) are also marked. Reconstructed possible area (dotted yellow line) of the HTPL according to the modern contour line of 1033 m asl.

on widely distributed paleo-lacustrine sediments along the Yellow River in the Hetao Basin (HTB) in northern China (Li et al., 2005; Chen et al., 2008a; Jia et al., 2016). As well as being the source and upper reaches of the Yellow River on the TP, the HTB is also linked to the Hexi Corridor, dunefields, and the Gobi Desert to its west, and dunefields and the Chinese Loess Plateau (CLP) to its south (Figure 1A) through fluvial and aeolian processes (Nie et al., 2015; Yang et al., 2018; Fan et al., 2022). Therefore, the evolution of the HTPL may shed light on that of the Yellow River, regional climatic change, and surface processes.

The timing and extent of the HTPL are under debate, especially due to results from different dating methods. ^{14}C dating suggests its formation in Marine Isotope Stage (MIS) 3 (Yang et al., 2018; Yang et al., 2020). Chen et al. (2008b) proposed that the HTPL had extended to the Jilantai (JLT) Basin, forming a JLT-HT mega-lake at ~100 ka based on quartz optically stimulated luminescence (OSL) dating, and the lake then reached its highest stand of 1080 m asl at ~50-60 ka. Jiang et al. (2012) proposed a closed HTPL at 145-100 ka (quartz OSL), which then outflowed after reaching 1046 m asl. Evidence from drill cores in the Ulan Buh dunefield also display a JLT during MIS 5e–5c (Chen et al., 2013; Li et al., 2014). Recent dating of quartz OSL and post-infrared infrared stimulated luminescence (post-IR IRSL, pIRIR) of K-feldspar (KF) from major shorelines in the JLT Basin further confirm paleo-lake development during MIS 5 (~1070 m asl) and MIS 3 (~1050–1060 m asl) (Fan et al., 2022).

It is unclear whether the inconsistency in the dating of the HTPL is due to the multiple stages of paleo-lake development or different

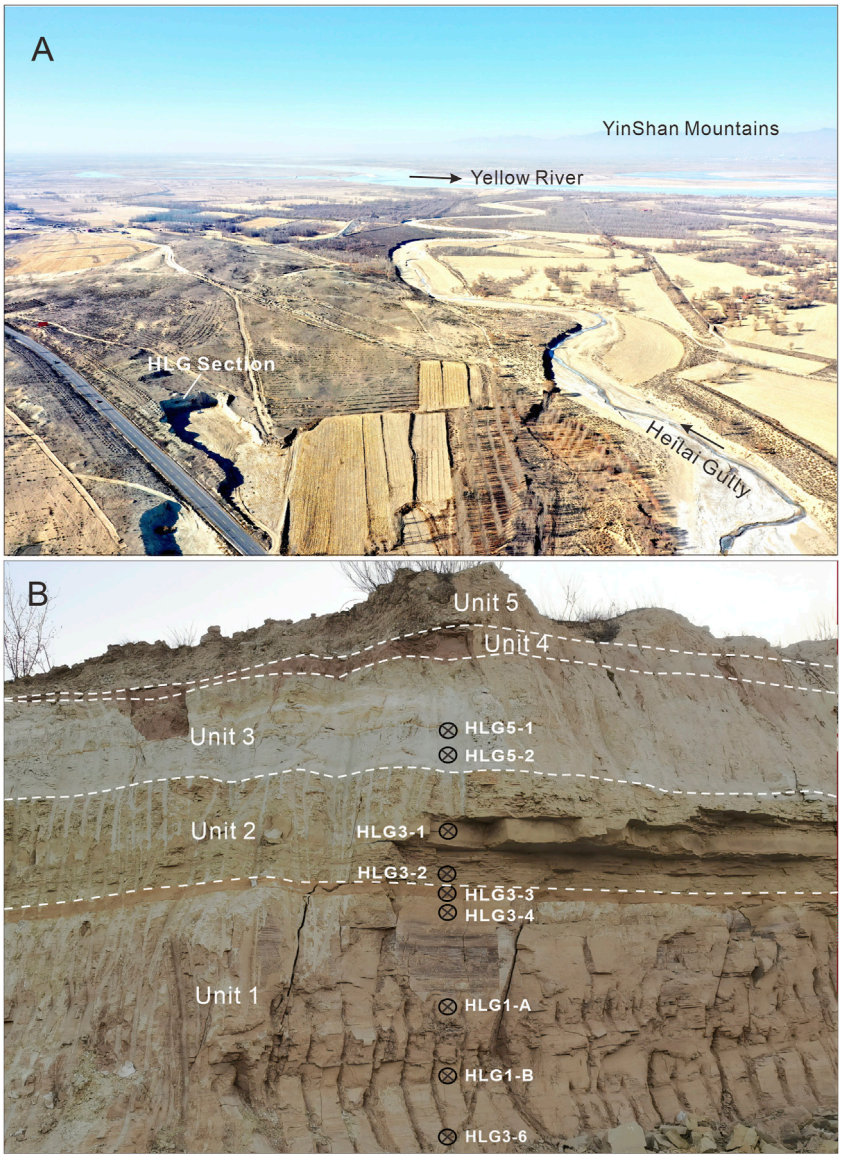

FIGURE 2
(A) Overview of modern environment in the study region; the Yellow River is 3 km north of the HLG section. **(B)** Stratigraphy and sampling locations of HLG section.

dating methods. ^{14}C dating is known to usually underestimate lacustrine sediments of over 30 ka due to contamination from younger carbon (Lai et al., 2014). In recent years, quartz OSL dating has also been found to saturate much earlier than previously realized—ca. 150 Gy in CLP (Buylaert et al., 2008; Chapot et al., 2012) and even below 100 Gy in Qaidam Basin (Yu et al., 2022). Alternatively, pIRIR dating of KF with a much higher dating limit (Li and Li, 2012) may contribute to these questions, which has been applied but limited to the JLT sub-basin in the HTB (Li et al., 2014; Fan et al., 2022), leaving the reliable chronology of the HTPL unsolved. In this study, 9.4-m-thick paleo-lacustrine sedimentary records at the middle of the HTB were studied to determine the time of the HTPL by comparing both quartz OSL and KF pIRIR dating, and to discuss the possible mechanisms for the formation of the HTPL.

2 Geographic setting and section

2.1 Geographic setting

The Hetao Basin, a Cenozoic faulted basin on the Ordos Plateau, is located along the end of the upper reaches of the Yellow River from Shizuishan to Togtoh (Figures 1A, B), with an area of ca. 28,000 km^2 and altitude of 900–1200 m (Li et al., 2017a). The HTB is composed of four sub-basins: Jilantai, Linhe, Baiyanhua, and Houbao (Figure 1B). Late Quaternary lacustrine sediments are widely distributed in the HTB and are usually covered by loess, aeolian sand, and alluvium. The landscapes along the Yellow River are mainly desert and desert steppe, with the mobile Hobq dunefield on its southern bank (Figure 1B). Many ephemeral tributaries have originated from the Ordos Plateau and flowed across the Hobq

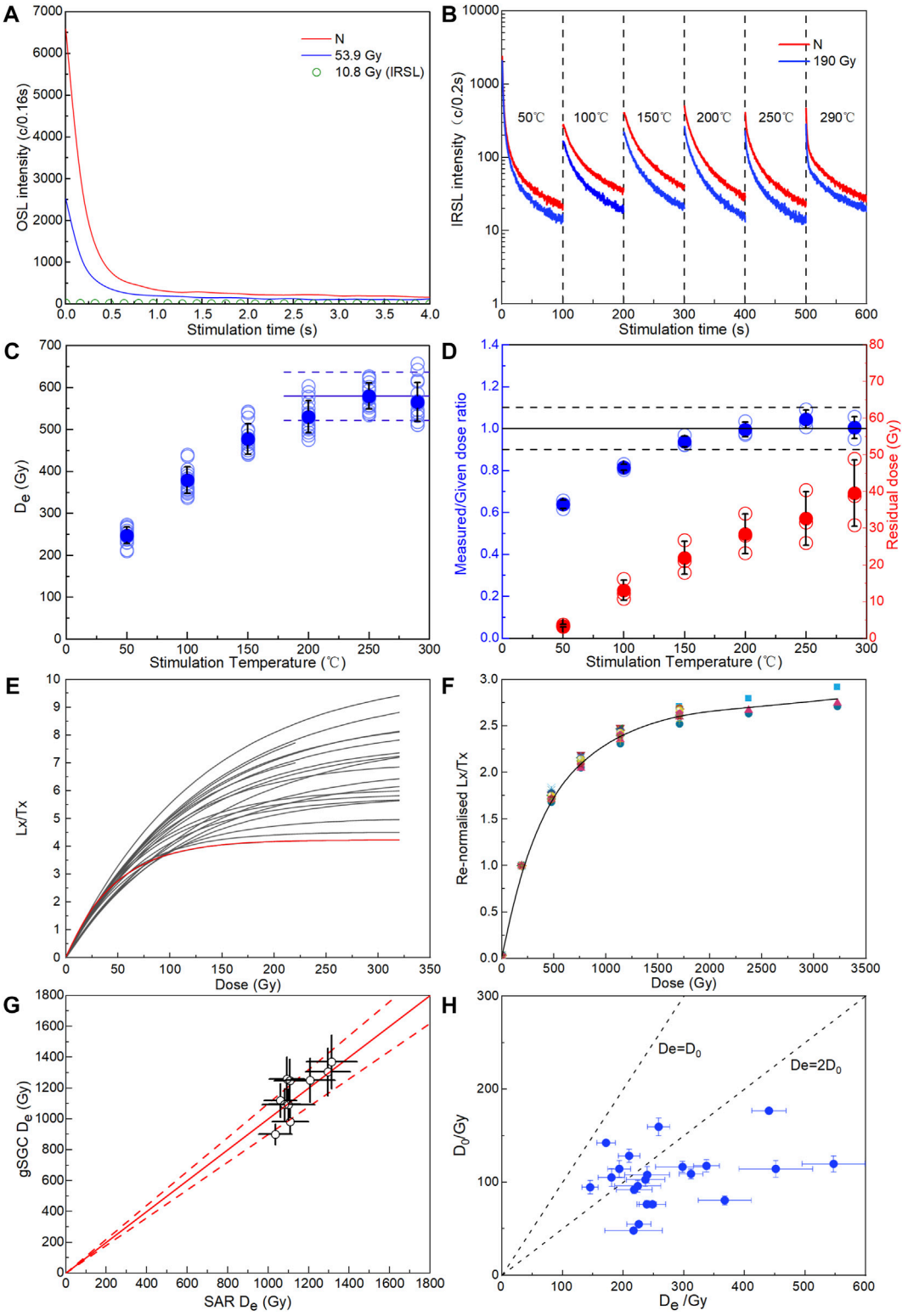

FIGURE 3
(A) OSL decay curves (HLG5-1). **(B)** Decay curves of MET-pIRIR signals (HLG5-1). **(C)** D_es at different stimulation temperatures (HLG5-1). **(D)** Dose recovery test of 237 Gy (blue) for MET-pIRIR protocols and residual doses after sunlight bleached under different stimulation for the MET-pIRIR signals of sample HLG5-2 (red). **(E)** All SAR dose response curves (DRCs) of measured quartz aliquots, which displayed different saturation levels. The lowest red curve displayed the aliquot with the lowest D_0 of only 48 Gy. **(F)** Renormalized DRCs (dots) and gSGC (solid line) of KF. **(G)** Comparisons of SAR D_es and gSGC D_es. **(H)** Relation of D_e *versus* D_0 in quartz aliquots.

dunefield, contributing sufficient material to the alluvial and pluvial processes in the HTB (Figure 1B).

The HTB lies along the margin of the EASM (Figure 1A) and has a semi-arid continental climate. Its annual mean temperature is 4°C–8°C, and annual mean precipitation is ca. 275 mm (mainly in summer) (Li et al., 2020a). However, its annual mean evaporation is ca. 1900–2500 mm (Wei et al., 2016), which far exceeds precipitation. Drought and large daily temperature ranges are typical climatic characteristics of the HTB. Under such a climate, local short, ephemeral tributaries make a limited contribution to the Yellow River in the HTB, and $^{87}Sr/^{86}Sr$ ratios of modern water samples suggest that the Yellow River was the dominant water source during the high lake phase (Fan et al., 2010). Additionally, the annual (1956–2017) mean runoff even decreases from 306×10^8 m^3 in Lanzhou to 208×10^8 m^3 in Togtoh (Figure 1A; Xie et al., 2021), suggesting that almost all the runoff to the HTB originates from the northeastern Tibetan Plateau.

2.2 Section and OSL sampling

Section Heilaigou (HLG, 40.46°N, 109.47°E, 1033 m asl.) is located near the mouth of the Heilai Gully and is about 20 m above the modern Yellow River (Figure 2A). This artificial section exposed a set of 9.4-m-thick lacustrine deposits (Figure 2B). The section was divided into five units from bottom to top according to sedimentary characteristics such as color, grain size, and bedding (Figure 2B).

Unit 1 (base not reached, 3.8 m) at the base of the section is mainly composed of well consolidated reddish-brown silty fine sand (Figure 2B). The obvious horizontal beddings of several centimeters thick suggest that they resulted from rapid deposition events, such as floods. There are no gravels in this unit and no desiccation crack on the fine-grained surface of each couplet, demonstrating that they were subaqueous deposits. Therefore, these sediments should be flood inputted shallow lacustrine deposits. The thick couplets suggest that these floods were mainly from the Heilai gully, and the reddish-brown coarse sand layer at the top of this unit may be attributed to an intensive flood event. Unit 2 (2.2 m) is composed of pale green silty sand with apparent dense horizontal beddings a few centimeters thick, suggesting a relatively deeper lake environment. Unit 3 (1.1 m) is composed of relatively loose grayish-white clayey silt and thin horizontal beddings, which also demonstrate a deep lacustrine environment. Unit 4 is reddish loose dune sand with obvious oblique beddings, and Unit 5 is sandy loess with dark soil later in the middle part. These two aeolian units are dated to the last Holocene deglaciation (unpublished data), implying that the lake level did not reach this elevation during this period. However, they are not relevant to the evolution of the HTPL and are therefore are not studied here.

Nine OSL samples were taken by stainless steel tubes from the three lacustrine units. The sampling locations are shown in Figure 2B. The OSL samples were taken by hammering stainless steel tubes (~25 cm long and ~5 cm diameter) into the freshly cleaned sections. Buck samples were also taken from some layers for grain size, organic material, and carbonate measurements.

3 Methods

3.1 Luminescence dating

3.1.1 Sample preparation and experimental equipment

The pretreatment and measurement of the nine OSL samples were carried out in the Luminescence Research Laboratories of Linyi University and Liaoning Normal University, China. About 2–3 cm of materials from both ends of the tubes were removed to measure grain size, elements, water, and carbonates, and the unexposed internal part was used for equivalent dose (D_e) determination. Grain size fractions of 63–90 μm or 125–180 μm (only for HLG3-3) were separated by wet sieving after successively removing the carbonates and organics with 10% HCl and 30% H_2O_2. Quartz and KF were extracted using heavy liquids with densities of 2.62–2.70 g/cm^3 and 2.53–2.58 g/cm^3, respectively. The quartz was then etched with 40% HF for about 40 min to dissolve feldspars and the alpha-irradiated outer layer (~10 μm), followed by HCl rinsing to remove fluorides. The KF was not etched (Duller, 1992). Aliquots with 2 mm diameters on stainless disks were used for both KF and quartz samples. Two samples were also measured by single-grain dating of KF.

All D_e measurements were performed on an automated luminescence reader (Risø TL/OSL-DA-20-D) equipped with a $^{90}Sr/^{90}Y$ beta source, blue (470 ± 20 nm), and infrared (870 ± 40 nm) diodes, and a X-Y single-grain device. The stimulated signals were counted by a PDM9107Q photomultiplier tube, after passing through a 7.5 mm thick U-340 filter (for quartz) or combined Schott BG39 and BG3 filters (for KF).

3.1.2 Luminescence characteristics and D_e determination

The single-aliquot regenerative-dose (SAR) protocol (Murray and Wintle, 2000; Murray and Wintle, 2003) and standard growth curve (SGC) method (Roberts and Duller, 2004) were used for D_e measurement of both quartz and KF. Five samples (HLG5-1, HLG5-2, HLG3-1, HLG3-4, and HLG3-6) were measured with quartz OSL. For quartz OSL, a modified SAR protocol (An et al., 2020) was referred to, with a preheating temperature of 260°C for 10 s and a cutting temperature of 220°C for 10 s; only the aliquots with very low IRSL signal contamination and low recuperation were used. OSL signals of the first 0.64 s stimulation were integrated for calculation after background (last 10 s) subtraction. Figure 3A shows the decay curves of quartz OSL signals (HLG5-1), which decayed quickly to the background level in the first second of stimulation, suggesting that the signals are dominated by fast components.

For KF single-aliquot D_e measurement, the multi-elevated-temperature (MET) pIRIR protocol (Li and Li, 2011; Li and Li, 2012) was used in this study. Samples were preheated to 320°C for 60 s, stimulated with IR for 100 s at 50, 100, 150, 200, 250, and 290°C, respectively, and bleached at 320°C after each nature/regeneration cycle (Yu et al., 2022). Figure 3B illustrates the decay curves of natural (red) and regenerative (blue) signals under different stimulation temperatures. The signals of the initial 8 s were used, and the last 10 s were subtracted as background (Yu et al., 2022). Figure 3C shows an obvious D_e plateau between 250°C and 290°C, indicating that the signals were well bleached and not significantly

TABLE 1 Dose rates of all quartz and KF samples.

Sample ID	Depth (m)	U (ppm)	Th (ppm)	K (%)	Water content (%)	Mineral (KF/Q)	Grain size (μm)	Cosmic dose rate (Gy/ka)	Internal dose rate (Gy/ka)	Total
HLG5-1	2.5	4.39 ± 0.18	4.73 ± 0.19	0.92 ± 0.04	10 ± 5	KF	63–90	0.24	0.264	3.21 ± 0.21
					10 ± 5	Q	63–90	0.24		2.31 ± 0.09
HLG5-2	2.8	5.33 ± 0.21	3.60 ± 0.14	0.71 ± 0.03	10 ± 5	KF	63–90	0.21	0.264	3.19 ± 0.24
					10 ± 5	Q	63–90	0.21		2.22 ± 0.09
HLG3-1	4	2.71 ± 0.11	9.85 ± 0.39	1.92 ± 0.08	10 ± 5	KF	63–90	0.15	0.264	3.96 ± 0.22
					10 ± 5	Q	63–90	0.15		3.10 ± 0.14
HLG3-2	4.9	3.60 ± 0.14	10.43 ± 0.42	1.82 ± 0.07	10 ± 5	KF	63–90	0.13	0.264	4.2 ± 0.24
HLG3-3	5.2	7.02 ± 0.28	5.94 ± 0.24	0.98 ± 0.04	10 ± 5	KF	125–180	0.13	0.525	3.87 ± 0.21
HLG3-4	5.9	2.89 ± 0.12	11.64 ± 0.47	2.17 ± 0.09	10 ± 5	KF	63–90	0.12	0.264	4.39 ± 0.24
					10 ± 5	Q	63–90	0.12		3.45 ± 0.15
HLG1-A	7.6	3.07 ± 0.12	11.49 ± 0.46	2.2 ± 0.09	10 ± 5	KF	63–90	0.1	0.264	4.44 ± 0.25
HLG1-B	8.6	3.75 ± 0.15	11.76 ± 0.47	2.04 ± 0.08	10 ± 5	KF	63–90	0.09	0.264	4.54 ± 0.26
HLG3-6	9.3	4.22 ± 0.17	12.11 ± 0.48	2.15 ± 0.09	10 ± 5	KF	63–90	0.09	0.264	4.80 ± 0.29
					10 ± 5	Q	63–90	0.09		3.71 ± 0.16

affected by anomalous fading (Li and Li, 2011; Fu, 2014). The residual dose test and dose recovery test were conducted on six solar bleached (5 days) aliquots (HLG5-2). Three of these were used to measure the residual dose, and the mean residual dose increased with stimulation temperatures: 32.7 ± 7.3 Gy and 39.5 ± 9.1 Gy at 250°C and 290°C, respectively (Figure 3D). A laboratory beta-dose of 231.8 Gy was irradiated to the other three aliquots. After subtracting the corresponding residual doses, the average dose recovery ratios (Figure 3D) under 250°C and 290°C were 1.04 ± 0.04 and 1.00 ± 0.05, respectively. This suggests that the MET-pIRIR procedure is suitable for KF in this region, and the signals of 250°C were used for D_e calculation. Two samples (HLG5-1 and HLG5-2) were measured using single-grain KF dating, with a two-step $pIR_{200}IR_{275}$ procedure (Li et al., 2018a). Individual KF grains were placed on single-grain discs with a hole diameter of 100 μm.

The dose response curves (DRC) of five quartz samples and nine KF samples were used to establish SGCs of quartz and KF, respectively. To further reduce the between-aliquot variation in SAR DRCs (Figure 3E), the "global" SGC (gSGC) method (Li et al., 2015a) was applied. Following the measurement of the natural signal, both the normalized nature signals and the DRCs were renormalized by extra regenerative doses (Li et al., 2015a; 2015b) of 189.8 Gy for KF and 53.9 Gy for quartz. A total of 21 quartz DRCs and 18 KF DRCs were used to build gSGCs, and Figure 3F shows the renormalized DRCs (dots) and gSGC (solid line) of KF. D_e values were obtained by matching the renormalized natural signals to the gSGC. Figure 3G demonstrate that the D_es obtained by gSGC and SAR are consistent for KF. The final D_es were calculated with the central age model (Galbraith et al., 1999).

3.1.3 Dose rate

The U and Th concentrations of each sample were measured by inductively coupled plasma mass spectrometry, while the content of K was measured by inductively coupled plasma optical emission spectrometry. The internal K content of KF was estimated as 12.5% ± 0.5% (Huntley and Baril, 1997). The α-value of coarse-grained KF is 0.15 ± 0.05 (Balescu and Lamothe, 1994). The cosmic dose rates were calculated according to Prescott and Hutton (1994). The water content was estimated as 10% ± 5% for the samples based on the measured values and the burial environment. The dose rates and ages were calculated with DRAC (v1.2) (Durcan et al., 2015) and

TABLE 2 Dating results of quartz OSL and KF MET-pIRIR.

Sample ID	Depth (m)	Mineral (KF/Q)	Dose rate (Gy/ka)	OD (%)	Aliquot/grain number	D_e (Gy)	Calibrated D_e (Gy)	Age (ka)
HLG5-1	2.5	KF, single-grain	3.21 ± 0.21	15.7	44	386 ± 13		120 ± 9
		Q	2.31 ± 0.09	28.7	14	238 ± 19		103 ± 9
HLG5-2	2.8	KF, single-grain	3.19 ± 0.24	24.8	58	384 ± 16		120 ± 10
		KF	3.19 ± 0.24	14.2	20	452 ± 15	419 ± 15	131 ± 12
		Q	2.22 ± 0.09	25.9	16	210 ± 14		95 ± 7
HLG3-1	4	KF	3.96 ± 0.22	15.8	22	1005 ± 39	972 ± 39	245 ± 17
		Q	3.10 ± 0.14	32.1	13	284 ± 28		92 ± 10
HLG3-2	4.9	KF	4.2 ± 0.24	13.7	17	1059 ± 44	1026 ± 44	244 ± 18
HLG3-3	5.2	KF	3.87 ± 0.21	20.8	19	1082 ± 58	1049 ± 58	271 ± 22
HLG3-4	5.9	KF	4.39 ± 0.24	11.1	13	1205 ± 53	1172 ± 53	267 ± 19
		Q	3.45 ± 0.15	20.5	11	337 ± 23		98 ± 8
HLG1-A	7.6	KF	4.44 ± 0.25	22.1	14	1170 ± 78	1137 ± 78	256 ± 23
HLG1-B	8.6	KF	4.54 ± 0.26	13.1	13	1187 ± 58	1154 ± 58	254 ± 20
HLG3-6	9.3	KF	4.80 ± 0.29	11.6	13	1319 ± 64	1287 ± 64	268 ± 21
		Q	3.71 ± 0.16	24.3	13	295 ± 21		80 ± 7

with the conversion factors of Adamiec and Aitken (1998). The dose rates for all samples are listed in Table 1.

3.2 Grain size and loss on ignition

The grain size of the samples was measured using a laser particle size analyzer (Bettersize 2600) at Linyi University with a measurement range of 0.02–2600 μm. Samples were pretreated and measured following the method proposed by Zhao et al. (2016). The contents of organic matter and carbonates were determined with the loss on ignition (LOI) method using a Muffle furnace at Linyi University. The dried (3 g, at 105°C for 12 h) samples were heated to 550°C for 3 h and then 950°C for 4 h to analysis the contents of organic matter and carbonates, respectively (Heiri et al., 2001).

4 Results

4.1 KF pIRIR and quartz OSL dating

The quartz OSL and KF pIRIR ages are shown in Table 2 and Figure 4. The concentrated D_es (Figure 5) and low over-dispersion (OD) values based on single-grains or small aliquots indicate homogeneous bleaching of pIRIR signals before burial. The five KF ages in Unit 1 range from 254 ± 20 ka to 276 ± 22 ka. The two samples from Unit 2 were dated at 245 ± 17 ka and 244 ± 18 ka, showing that they were deposited in early MIS 7. Unit 3 yielded two single-grain KF ages of 120 ± 9 ka and 120 ± 10 ka and one single-aliquot KF age of 131 ± 12 ka, suggesting that this unit was mainly formed during ca. 120–130 ka—the MIS 5e. The consistent single-grain and single-aliquot ages suggest that the signals are well bleached and the ages are reliable. It is worth noting that there is an obvious sedimentary hiatus of ca. 110 ka between the two stages of HTPL development. In contrast, the ages of the five quartz samples ranged from 80 ± 7 ka to 103 ± 9 ka, which cannot correspond to the stratigraphy (Figure 4).

4.2 Grain size and LOI

The frequency-distribution curves of the grain sizes of lacustrine and aeolian sediments from the HLG section are shown in Figure 6. The results show that the grain-size composition of the different lacustrine units vary significantly, suggesting a different sedimentary environment. The curves of Unit 1 show characteristics of poorly sorted flood deposits (Liu et al., 2019) with many peaks (Figure 6A), which suggest an unstable sedimentary environment. Unit 2 has coarser grain size than Unit 1, with less clay to fine silt and more coarse silt to very fine sand (Figure 6B). The dominant coarser component is close to the dune sand in Unit 4 and sandy loess in Unit 5 (Figure 6D). The grain size of Unit 3 is relatively finer than Unit 2, suggesting a deeper lake with a stable sedimentary environment and less aeolian input (Figure 6C).

Organic matter content varies from 2.17% to 22.76%, with the highest contents occurring in Unit 3 (Figure 4). The content of carbonates is converted to $CaCO_3$ based on the LOI under 950°C. The content of $CaCO_3$ increases from Unit 2 in response to the rising lake level, and the highest contents (42.3% in average) occur in Unit 3 (Figure 4). Therefore, grain size and organic matter and

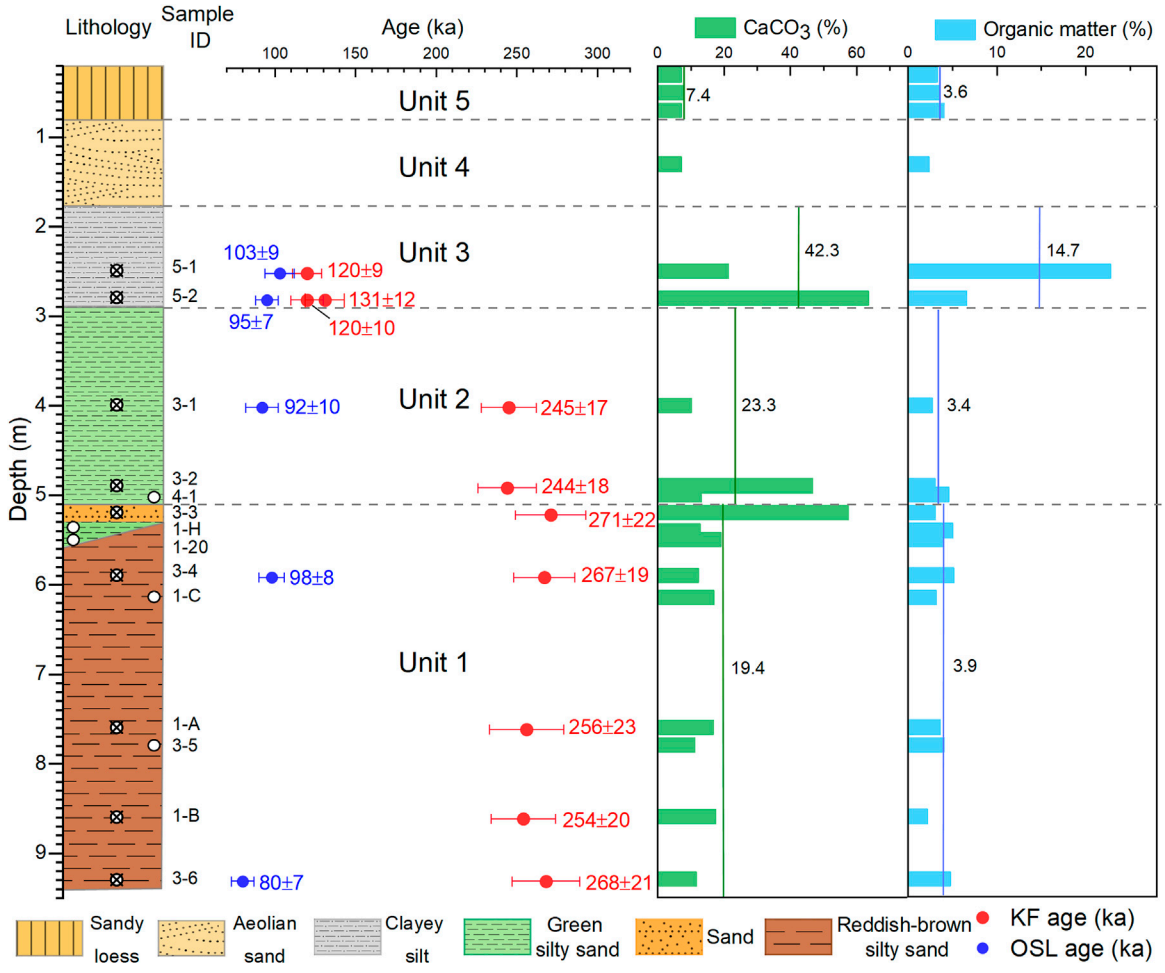

FIGURE 4
Lithological characteristics, quartz OSL, and KF MET-pIRIR ages and contents of carbonates and organic matter in HLG section.

carbonate content all suggest that Units 2 and 3 were deposited under a deep lake environment, especially Unit 3.

5 Discussion

5.1 Upper limit of quartz OSL dating in HTB

A comparison of KF pIRIR and quartz OSL ages in the HLG section reveals disagreement (Table 2). The OSL ages of the five samples vary between 80 and 103 ka, and they do not increase with depth like the pIRIR ages, which yield a consistent sequence from 120 ka to 268 ka. Considering that the residual dose (32.7 Gy) of the pIRIR signals have been subtracted, we attribute this disagreement to the underestimation of quartz OSL ages. The D_0 values range from 48 Gy to 177 Gy, with an average value of 106 Gy. The red line in Figure 3E illustrates one of the earliest saturated quartz DRC, which has a D_0 of only 48 Gy; Figure 3H demonstrates that D_es of almost all the quartz aliquot measured with SAR protocol (141–547 Gy) are close to or exceed the average saturation level of 2 D_0 (Wintle and Murray, 2006). Some individual grains saturated even before 96 Gy (ca. 32 ka with an average dose rate of ca. 3 Gy/ka in HTB). These early-saturated grains may affect the results of the whole aliquots, even though the aliquots may have a higher saturation level (Yu et al., 2022). Additionally, according to the study of loess-paleosoil sequences on the CLP, although the DRCs may have a higher saturation level, the natural signals saturate much earlier, at ca. 150 Gy (Chapot et al., 2012). This offers another interpretation of the underestimation of aliquots with D_es of lower than 2 D_0. Therefore, most quartz aliquots in this study should have been affected by signal saturation.

Fan et al. (2020) also suggested that the quartz in the JLT sub-basin, southwestern HTB, saturated at ca. 150 Gy. Many other studies have demonstrated that quartz in the arid and semi-arid regions and the TP in China has a much lower saturation level than previously thought, such as loess in the western CLP (150 Gy, Buylaert et al., 2008; Wang et al., 2018), Tianshan (125 Gy, Li et al., 2016), and shorelines in the Gaxun Nur Basin (132 Gy, Li et al., 2017b). Additionally, according to the detailed comparisons between quartz OSL and KF MET-pIRIR ages of aeolian and fluvial sediment in the Qaidam Basin by Yu et al. (2022), even though the values of 2 D_0 varied between 90 and 240 Gy (184 Gy on average),

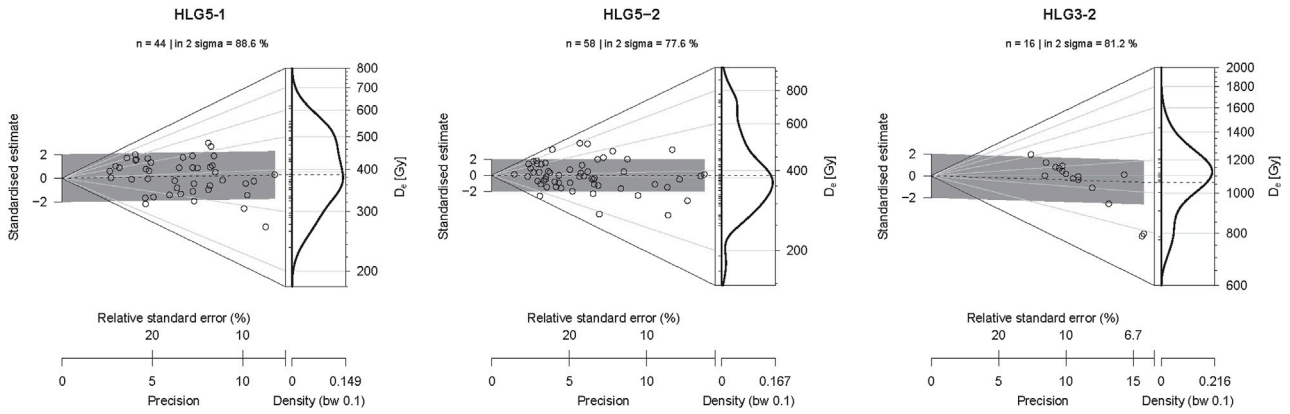

FIGURE 5
D_e distribution of KF samples measured with single-grain (HLG5-1 and HLG5-2) and single aliquot (HLG3-2).

the effect of saturation may occur as early as 74 Gy (27.5 ka, with corresponding pIRIR age of 42 ka).

In contrast, the pIRIR dating usually has a much higher saturation level (Thiel et al., 2011; Buylaert et al., 2012), supporting studies of mega-lake evolution since MIS 7 or MIS 9 in, for example, the Ejina (Li et al., 2018b) and the Qaidam Basins (Cao et al., 2021; Ding et al., 2021). In this study, the D_es of the MET-pIRIR range from 384 to 1319 Gy, with most within 2 D_0. Even if the ages with relative higher D_es of ca. over 1000 Gy may be affected by saturation, this may not change the pattern of the HTPL occurring during MIS 7 and MIS 5.

5.2 Evolution of the HTPL during MIS 7 and MIS 5

According to the chronological and sedimentological analysis, the paleo-lacustrine records in the HLG section demonstrate two stages of HTPL.

Stage I: early MIS 7. Although the five KF ages in Unit 1 correspond within errors, in consideration of the worse bleaching of flood origin sediments (An et al., 2020; Liu, 2020 ; Yang et al., 2022) and feldspar, we suggest taking an average of the two youngest ages (254 ± 20 ka and 256 ± 23 ka)—255 ± 23 ka—which is almost the same as that of Unit 2—245 ± 18 ka. This suggests that the two distinct units were deposited within a short period: the early stage of MIS 7. Unit 1 suggests a shallow lake with a high depositional rate (thick coarse-fine couplets of over 10 cm, oxidizing environment). The discontinuity of the greenish layer and the occurrence of the overlying coarse-grained sandy flood layer suggest fluctuation of the lake level. Unit 2 suggests a deeper lacustrine environment with low sedimentary rate, as revealed by thin horizontal beddings and high carbonate contents (Figure 4). The higher aeolian dust input (coarser silt to very fine sand, Figure 6B) also demonstrates decreased fluvial input under a highstand. Therefore, the sedimentary characteristics reveal abrupt lake level rise (to over 1033 m asl) during the early MIS 7.

Stage II: early MIS 5. The two ages constrain the formation of the last stage of the dated mega-lake to the early MIS 5. The white color, high content of organic materials and carbonates, and the finest grain-size composition all demonstrate that the lake level during MIS 5 was higher than that of MIS 7—much higher than 1033 m asl.

At present, the KF pIRIR dating has confirmed the existence of a mega JLT paleo-lake during MIS 3 and MIS 5 (Fan et al., 2022). In this study, our MET-pIRIR$_{250}$ ages also confirms the existence of a mega-lake in the HTP during MIS 5 and further extends its existence to MIS 7 for the first time. Although the HTPL has been dated to different stages by quartz or ^{14}C (Li et al., 2005.; Chen et al., 2008a; Jiang et al., 2012; Jia et al., 2016; Yang et al., 2018; Yang et al., 2020), this might be difficult to compare with the new KF pIRIR ages (this study; Fan et al., 2022) because ^{14}C usually underestimates lacustrine sediments beyond 30 ka (Lai et al., 2014) while this study finds that quartz OSL may also subject to saturation when over 96 Gy, which equals ca. 32 ka for lacustrine samples with average dose rate of 3 Gy/ka in the HTB. In this case, most former ages of the HTPL dating to over 30 ka by quartz OSL or ^{14}C may need further re-evaluation. For example, the quartz OSL ages of ~145–100 ka, which suggested HTPL formation during MIS 5, had D_es of ca. 280–310 Gy (Jiang et al., 2012), and were very likely underestimated. In addition, lacustrine sediments of the same stages may occur at any elevation below the lake level—for example, lacustrine sediments dated to MIS 5 were reported at 1070 m asl (Fan et al., 2022), 1050–1080 m, etc. (Li et al., 2005) and 1033 m asl (this study). Therefore, we may only estimate the minimal scale (~14,470 km^2, Figure 1B) of the HTPL based on its minimal elevation of 1033 m asl at present, if the topographic changes since MIS 7 are not considered. Additionally, without exact lake level elevation, a detailed chronology of lacustrine strata in the Dengkou Uplift area (Figure 1B), and a reliable estimate of the extent of the Ulan Buh dunefield, the relationship between the HTPL and JLT paleo-lake during these stages remains unclear. Further chronological studies by, for example, KF pIRIR dating of lacustrine sediments or shorelines in multiple sites will be needed to reconstruct the scale of the paleo-lake in the whole HTB.

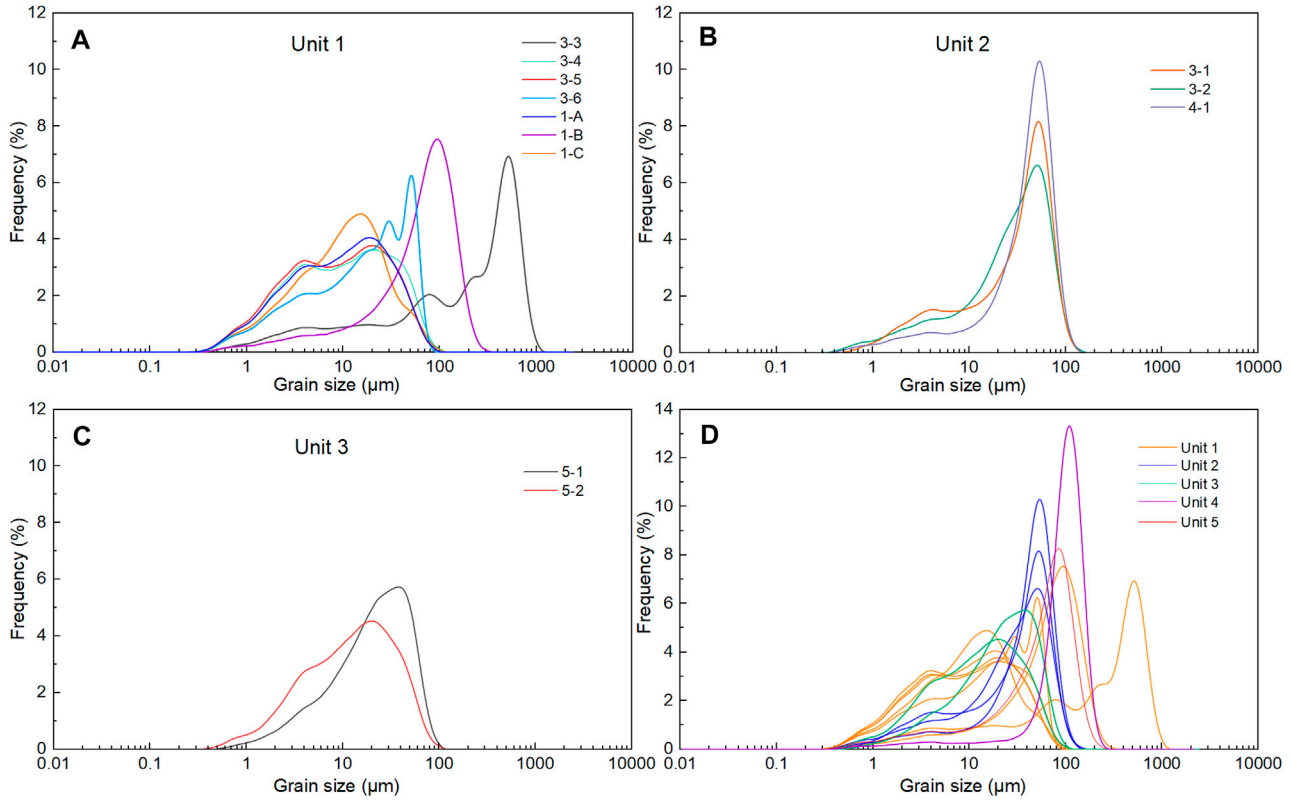

FIGURE 6
Grain-size frequency distribution of lacustrine samples from lacustrine Units 1–3 **(A–C)** and their comparisons with aeolian sand and sandy loess in Units 4 and 5 **(D)**.

5.3 Possible mechanisms for the formation of the HTPL

After the Jin-shaan Gorge was cut through at ca. 1.2 Ma, the HTB was connected to the modern Yellow River, which gradually drained its original lake (Pan et al., 2009; 2011; Jia et al., 2016; Li et al., 2017a). However, thereafter the mega-lake resumed occasionally since at least mid-Pleistocene (Li et al., 2005.; Li et al., 2007; Chen et al., 2008a; Jiang et al., 2012; Jia et al., 2016; Yang et al., 2018; 2020; Li et al., 2020a; Fan et al., 2020). This requires the closure of the HTB and an adequate water supply. Tectonic activity and climatic change are widely accepted as the dominant mechanisms (Chen et al., 2013; Wei et al., 2016). Here, we discuss the possible mechanisms for the resuming of the HTPL.

5.3.1 Climatic change

There is almost no dispute on the water supply for the formation of the HTPL. Former studies proposed that abundant precipitation from the strong ASM was the main factor for the paleo-lake development in the HTB during MIS 3 and MIS 5 (Chen et al., 2008b; Cheng et al., 2016; Wei et al., 2016; Fan et al., 2022). Our new KF pIRIR ages constrain the development of HTPL to the early stage of MIS 7 and MIS 5 (Figure 7A), when the ASM was enhanced (Figure 7B; Cheng et al., 2016) under relative higher isolation (Figure 7C; Berger and Loutre, 1991) and higher sea level (Figure 7D; Spratt and Lisiecki, 2016). Climate in the northeastern TP and the western CLP—the main water source for the upper Yellow River—has been proven to be humid during MIS 7 and MIS 5 by loess studies (Li et al., 2020b; Sun et al., 2021 (Figures 7E, F)) and lacustrine sediments (Cao et al., 2021; Ding et al., 2021). The timing of the beginning of interglacial periods also suggests that increased meltwater from source regions on the TP during deglaciation also contributed to the evolution of the mega-lakes (Ding et al., 2021; Huang et al., 2023).

5.3.2 Damming of the HTB

The re-damming of the HTB, was previously attributed to tectonic uplift (Chen et al., 2008b; Li et al., 2020a), such as the formation of the HTPL during MIS 5e-5c being attributed to the rapid tectonic uplift at the northeastern margin of the Ordos Plateau (Chen et al., 2008b). Although a tectonic uplift event at ca. 100 ka has been proposed based on stratigraphic records from the ZKHB and Haojiayao cores (Figure 1B) in the eastern HTB (Li et al., 2007; Jiang et al., 2012), robust chronology and some crucial information such as the location and extent of the uplift are still needed to directly link tectonic activity to the close of the HTB.

In addition to tectonic uplift, we propose an alternative hypothesis for the closure of the HTB: it might have been dammed by accumulation of dunes at the northern end of the

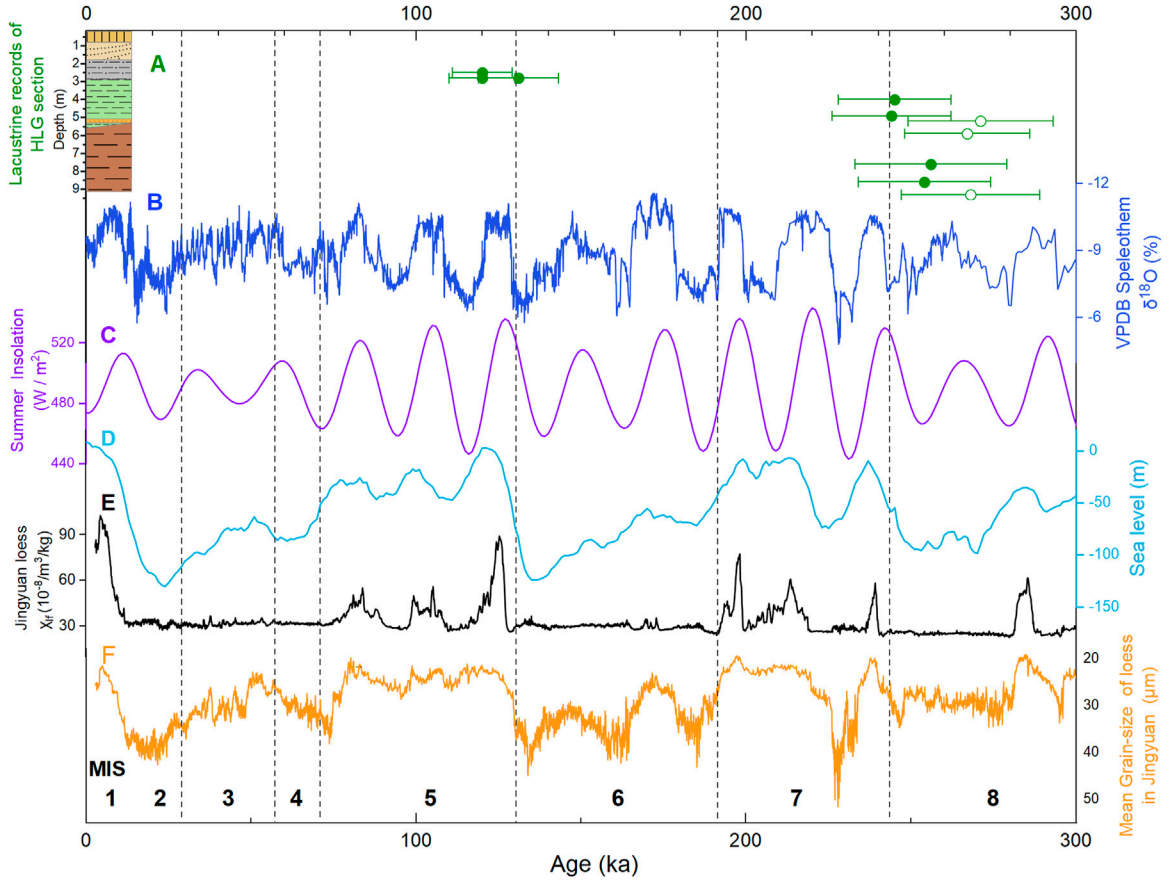

FIGURE 7
Comparison of **(A)** formation time of HTPL with **(B–F)** regional and global climatic records. Legends of A are the same as those in Figure 4, and ages marked with green circles are not used. **(B)** δ18O records of cave stalagmites in regions controlled by ASM (Cheng et al., 2016). **(C)** Summer solar insolation at 30° N (Berger and Loutre, 1991). **(D)** Sea level change (Spratt and Lisiecki, 2016). **(E)** Magnetic susceptibility and **(F)** mean grain-size records of Jingyuan loess from the northeastern CLP (Sun et al., 2021).

Jin-Shaan Gorge (Figure 8). Plentiful sedimentological evidence from the HTB indicates that the development of the HTPL is characterized by the alternation of geomorphic landscapes such as rivers, deserts, and lakes (Li et al., 2007; Li et al., 2014; Li et al., 2017a). This suggests that the evolution of the HTPL might be associated with aeolian–fluvial interaction (Yu et al., 2022). Dune damming plays a crucial role in blocking the extension of rivers and trapping water in lakes, and is more common in arid and semi-arid regions (Magaritz and Enzel, 1990; Ben-David, 2003). Not only have some small-scale ephemeral streams like Wadi Ruth in the Negev Dunefield and the Tiekui River in the Qaidam Basin been dammed by dunefield expansion (Roskin et al., 2017; Robins et al., 2022; Yu et al., 2022), but large rivers such as the Nile could also have been dammed by the expanded Sahara (Vermeersch and Neer, 2015).

The two stages of HTPL development in the early MIS 7 and MIS 5 demonstrate their strong linkage to glacial-scale climatic changes. The height of the valley shoulder of the Jin-Shaan Gorge provides favorable terrain conditions for the construction of a dune dam. Under the cold and arid climate during MIS 8 and MIS 6 (Figure 8), the Hobq dunefield might have expanded eastwards to accumulate in the Jin-Shaan Gorge, resulting in the damming of the HTB. On the other hand, the Yellow River might have frequently dried-up and therefore had insufficient flow to remove the accumulated dune sand in the Jin-Shaan Gorge. Then, during subsequent deglaciation, dunefield accumulation/expansion might have continued (Lu et al., 2013; Xu et al., 2015; Yu et al., 2015; 2022) with increased fluvial-sourced sand supply and strong wind (Yu et al., 2022), further facilitating the damming of the gorge. The sufficient water supply from increased precipitation and glacial meltwater during the humid MIS 7 and MIS 5, including the deglaciation periods before them, may have resulted in a quick rise of the lake level; when it exceeded the dune dam, the HTPL may have overspilled and caused dune dam breaching. Unconsolidated dune sand facilitates a quick dam breach, resulting in an abrupt disappearance of the mega-lake. Therefore, damming and breaching in the Jin-Shaan Gorge could well explain the multistage formation of the HTPL, especially its close association with climatic change on the glacial-interglacial scale. Further sedimentological and chronological evidence is needed to support this hypothesis.

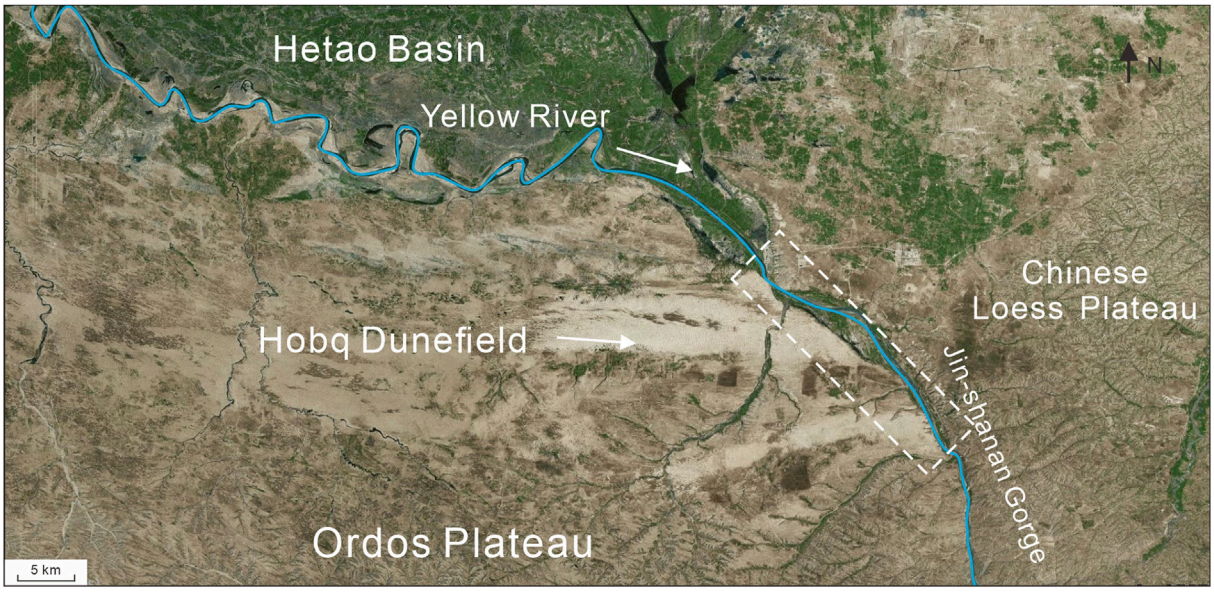

FIGURE 8
Entrance of the Jin-shanan Gorge, where the Yellow River might have been dammed by the Hobq dunefield in some narrow places (white square).

6 Conclusion

Lacustrine sediments were dated by quartz OSL and KF MET-pIRIR to determine the formation time of the Hetao paleo-lake (HTPL) in the Hetao Basin (HTB). Two main conclusions were drawn: one is the methodology of luminescence dating, and the other is related to the region's geomorphic processes. The OSL ages from quartz are underestimated due to signal saturation (as low as 96 Gy for some quartz aliquots). Therefore, KF pIRIR dating is used to cross-check with quartz OSL ages for samples older than MIS 3. KF dating results show that HTPL experienced two apparent highstand periods (over 1033 m) during the early MIS 7 (255–245 ka) and early MIS 5 (130–120 ka). However, these data are not sufficient to demonstrate the scale of the HTPL and its relationship with the JLT paleo-lake. We propose an alternative hypothesis to explain the periodic occurrence of the HTPL and its strong linkage to glacial-scale climatic changes. The HTB was closed because the northern end of the Jin-Shaan Gorge was dammed by the expanded Hobq dunefield during cold and arid glacial periods, and then the HTPL formed quickly in response to increased glacial meltwater and precipitation on the northeastern Tibetan Plateau at the beginning of interglacial periods. The subsequent breaching of the loose dune dam might have terminated the development of the HTPL when the lake level exceeded the outlet of the dune dam.

Data availability statement

The original contributions presented in the study are included in the article/Supplementary Material; further inquiries can be directed to the corresponding author.

Author contributions

JL: investigation, writing—original draft, resources, and validation. HF: investigation, visualization, writing—original draft, and formal analysis. PA: formal analysis and investigation. HW: investigation. LY: conceptualization, investigation, validation, methodology, writing—review and editing, resources, supervision, project administration, and funding acquisition.

Funding

This study was supported by NSFC (41761144073, 41672167 and 41462006) and the Project of Introducing and Cultivating Young Talent in the Universities of Shandong Province (No. LUJIAOKEHAN-2021-51, granted to LY).

Acknowledgments

The authors thank Xiaodong Miao for English language editing and the two reviews for the comments.

Conflict of interest

The authors declare that the research was conducted in the absence of any commercial or financial relationships that could be construed as a potential conflict of interest.

Publisher's note

References

Adamiec, G., and Aitken, M. (1998). Dose-rate conversion factors: Update. *Anc. TL* 16, 37–50.

An, P., Yu, L. P., Wang, Y. X., Miao, X. D., Wang, C. S., Lai, Z. P., et al. (2020). Holocene incisions and flood activities of the Keriya River, NW margin of the Tibetan plateau. *Asian Earth Sci.* 191, 104224. doi:10.1016/j.jseaes.2019.104224

Balescu, S., and Lamothe, M. (1994). Comparison of TL and IRSL age estimates of feldspar coarse grains from waterlain sediments. *Quat. Sci. Rev.* 13, 437–444. doi:10.1016/0277-3791(94)90056-6

Ben-David, R. (2003). *Changes in desert margin environments during the climate changes of the Upper Quaternary*. Ph.D. Thesis. Jerusalem: Hebrew University of Jerusalem, 170. (Unpublished, in Hebrew).

Berger, A., and Loutre, M. F. (1991). Insolation values for the climate of the last 10 million years. *Quat. Sci. Rev.* 10, 297–317. doi:10.1016/0277-3791(91)90033-q

Buylaert, J. P., Murray, A. S., Vandenberghe, D., Vriend, M., De Corte, F., and Van den haute, P. (2008). Optical dating of Chinese loess using sand-sized quartz: Establishing a time frame for Late Pleistocene climate changes in the Western part of the Chinese Loess Plateau. *Quat. Geochronol.* 3, 99–113. doi:10.1016/j.quageo.2007.05.003

Buylaert, J. P., Jain, M., Murray, A. S., Thomsen, K. J., Thiel, C., and Sohbati, R. (2012). A robust feldspar luminescence dating method for Middle and Late Pleistocene sediments. *Boreas* 41, 435–451. doi:10.1111/j.1502-3885.2012.00248.x

Cao, M., Yu, L. P., An, P., Dong, Z. B., Zhao, J., Lai, Z. P., et al. (2021). Luminescence chronology and environmental implications of palaeolacustrine sediments beneath linear dunes in northern Qarhan Salt Lake region. *J. Desert Res.* 41, 101–110. (In Chinese). doi:10.7522/j.issn.1000-694X.2020.00102

China Earthquake Administration (CEA) (1988). *Active faults surrounding Ordos platea*. Beijing: Seismological Press, 20–75. (In Chinese).

Chapot, M. S., Roberts, H. M., Duller, G. A. T., and Lai, Z. P. (2012). A comparison of natural- and laboratory-generated dose response curves for quartz optically stimulated luminescence signals from Chinese Loess. *Radia Meas.* 47, 1045–1052. doi:10.1016/j.radmeas.2012.09.001

Chen, F. H., Fan, Y. X., Chun, X., Madsen, D. B., Oviatt, C. G., Zhao, H., et al. (2008a). Preliminary research on megalake jilantai-hetao in the arid areas of China during the late quaternary. *Chin. Sci. Bull.* 53, 1725–1739. doi:10.1007/s11434-008-0227-3

Chen, F. H., Fan, Y. X., Madsen, D. B., Chun, X., Zhao, H., and Yang, L. P. (2008b). Preliminary study on the formation mechanism of the "Jilantai-Hetao" megalake and the lake evolutionary history in Hetao region. *Quat. Sci.* 28, 866–873. doi:10.3724/SP.J.1047.2008.00014

Chen, F. H., Li, G. Q., Zhao, H., Jin, M., Chen, X. M., Fan, Y. X., et al. (2013). Landscape evolution of the ulan Buh desert in northern China during the late quaternary. *Quat. Res.* 81, 476–487. doi:10.1016/j.yqres.2013.08.005

Cheng, H., Edwards, R. L., Sinha, A., Spotl, C., Yi., L., Chen, S. T., et al. (2016). Correction: Corrigendum: The Asian monsoon over the past 640,000 years and ice age terminations. *Nature* 541, 122. doi:10.1038/nature20585

Ding, Z. J., Yu, L. P., Lai, Z. P., An, P., Miao, X. D., Xu, R. R., et al. (2021). Post-IR irsl chronology of paleo-lacustrine sediments from yardangs in the Qaidam Basin, NE Tibetan plateau. *Geochronometria* 48, 313–324. doi:10.2478/geochr-2020-0016

Duller, G. A. T. (1992). Comparison of equivalent doses determined by thermoluminescence and infrared stimulated luminescence for dune sands in New Zealand. *Quat. Sci. Rev.* 11, 39–43. doi:10.1016/0277-3791(92)90040-f

Durcan, J. A., King, G. E., and Duller, G. A. T. (2015). Drac: Dose rate and age calculator for trapped charge dating. *Geochronol.* 28, 54–61. doi:10.1016/j.quageo.2015.03.012

Fan, Y. X., Chen, F. H., Wei, G. X., Madsen, D. B., Oviatt, C. G., Zhao, H., et al. (2010). Potential water sources for Late Quaternary Megalake Jilantai-Hetao, China, inferred from mollusk shell 87Sr/86Sr ratios. *J. Paleolimnol.* 43, 577–587. doi:10.1007/S10933-009-9353-4

Fan, Y. X., Li, Z. J., Yang, G. L., Yi, S. W., Zhang, Q. H., Liu, W. H., et al. (2020). Sedimentary evidence and luminescence and ESR dating of Early Pleistocene high lake levels of Megalake Tengger, northwestern China. *J. Quat. Sci.* 35, 994–1006. doi:10.1002/jqs.3246

Fan, Y. X., Li, Z. J., Cai, Q. S., Yang, G. L., Zhang, Q. S., Zhao, H., et al. (2022). Dating of the late Quaternary high lake levels in the Jilantai area, northwestern China, using optical luminescence of quartz and K-feldspar. *Asian Earth Sci.* 224, 105024. doi:10.1016/j.jseaes.2021.105024

Fu, X. (2014). The De (T, t) plot: A straightforward self-diagnose tool for post-IR IRSL dating procedures. *Geochronometria* 41, 315–326. doi:10.2478/s13386-013-0167-9

Galbraith, R. F., Roberts, R. G., Laslett, G. M., Yoshida, H., and Olley, J. M. (1999). Optical dating of single and multiple grains of quartz from jinmium rock shelter, northern Australia: Part I, experimental design and statistical models. *Archaeometry* 41, 339–364. doi:10.1111/j.1475-4754.1999.tb00987.x

Heiri, O., Lotter, A. F., and Lemcke, G. (2001). Loss on ignition as a method for estimating organic and carbonate content in sediments: Reproducibility and comparability of results. *J. Paleolimnol.* 25, 101–110. doi:10.1023/A:1008119611481

Huang, C., Yu, L. P., and Lai, Z. P. (2023). Holocene millennial lake-level fluctuations of lake Nam Co in Tibet using OSL dating of shorelines. *J. Hydrology* 618, 128643. doi:10.1016/j.jhydrol.2022.128643

Huntley, D. J., and Baril, M. R. (1997). The K content of the K-feldspars being in measured in optical and thermoluminescence dating. *Anc. TL* 15, 11–13.

Jia, L. Y., Zhang, X. J., Ye, P. S., Zhao, X. T., He, Z. X., He, X. L., et al. (2016). Development of the alluvial and lacustrine terraces on the northern margin of the Hetao Basin, inner Mongolia, China: Implications for the evolution of the Yellow River in the Hetao area since the late pleistocene. *Geomorphology* 263, 87–98. doi:10.1016/j.geomorph.2016.03.034

Jiang, F. C., Wang, S. B., Li, C. Z., Fu, J. L., and Yan, H. (2012). On study of lacustrine formation and its meaning in the Togtoh platform, Inner Mongolia. *Quat. Sci.* 32, 931–937. (In Chinese). doi:10.3969/j.issn.1001-7410.2012.05.10

Lai, Z. P., Mischke, S., and Madsen, D. B. (2014). Paleoenvironmental implications of new OSL dates on the formation of the "shell bar" in the Qaidam Basin, northeastern qinghai-Tibetan plateau. *J. Paleolimnol.* 51, 197–210. doi:10.1007/s10933-013-9710-1

Li, B., and Li, S. H. (2011). Luminescence dating of K-feldspar from sediments: A protocol without anomalous fading correction. *Quat. Geochronol.* 6, 468–479. doi:10.1016/j.quageo.2011.05.001

Li, B., and Li, S. H. (2012). Luminescence dating of Chinese loess beyond 130 ka using the non-fading signal from K-feldspar. *Quat. Geochronol.* 10, 24–31. doi:10.1016/j.quageo.2011.12.005

Li, J. B., Ran, Y. K., and Guo, W. S. (2005). Research on the lacustrine strata of the tuoketuo mesa, Hetao Basin, China. *Quat. Sci.* 25, 630–639. (In Chinese). doi:10.3321/j.issn:1001-7410.2005.05.012

Li, J. B., Ran, Y. K., and Guo, W. S. (2007). Division of quaternary beds and environment evolution in hubao basin in China. *Quat. Sci.* 27, 632–644. (In Chinese). doi:10.1016/S1872-5791(07)60044-X

Li, G. Q., Jin, M., Wen, L. J., Zhao, H., Madsen, D., Liu, X. K., et al. (2014). Quartz and K-feldspar optical dating chronology of eolian sand and lacustrine sequence from the southern Ulan Buh Desert, NW China: Implications for reconstructing late Pleistocene environmental evolution. *Palaeogeogr. Palaeocl.* 393, 111–121. doi:10.1016/j.palaeo.2013.11.003

Li, B., Roberts, R. G., Jacobs, Z., and Li, S. H. (2015a). Potential of establishing a 'global standardised growth curve' (gSGC) for optical dating of quartz from sediments. *Quat. Geochronol.* 27, 94–104. doi:10.1016/j.quageo.2015.02.011

Li, B., Roberts, R. G., Jacobs, Z., Li, S. H., and Guo, Y. J. (2015b). Construction of a 'global standardised growth curve' (gSGC) for infrared stimulated luminescence dating of K-feldspar. *Geochronol.* 27, 119–130. doi:10.1016/j.quageo.2015.02.010

Li, G. Q., Rao, Z. G., Duan, Y. W., Xia, D. S., Wang, L. B., Madsen, D. B., et al. (2016). Paleoenvironmental changes recorded in a luminescence dated loess/paleosol sequence from the Tianshan Mountains, arid central Asia, since the Penultimate Glaciation. *Earth Planet Sci. Lett.* 448, 1–12. doi:10.1016/j.epsl.2016.05.008

Li, B. F., Sun, D. H., Xu, W. H., Wang, F., Liang, B. Q., Ma, Z. W., et al. (2017a). Paleomagnetic chronology and paleoenvironmental records from drill cores from the Hetao Basin and their implications for the formation of the Hobq Desert and the Yellow River. *Quat. Sci. Rev.* 156, 69–89. doi:10.1016/j.quascirev.2016.11.023

Li, G. Q., Li, F. L., Jin, M., She, L., Duan, Y., Madsen, D., et al. (2017b). Late Quaternary Lake evolution in the Gaxun Nur basin, central Gobi Desert, China, based on quartz OSL and K-feldspar pIRIR dating of paleoshorelines. *Quat. Sci.* 32, 347–361. doi:10.1002/jqs.2928

Li, B., Jacobs, Z., Roberts, R. G., and Li, S. H. (2018a). Single-grain dating of potassium-rich feldspar grains: Towards a global standardised growth curve for the post-IR IRSL signal. *Quat. Geochronol.* 45, 23–36. doi:10.1016/j.quageo.2018.02.001

Li, G. Q., Madsen, D. B., Jin, M., Stevens, T., Tao, S. X., She, L. L., et al. (2018b). Orbital scale lake evolution in the Ejina Basin, central Gobi Desert, China revealed by K-feldspar

luminescence dating of paleolake shoreline features. *Quatern. Int.* 482, 109–121. doi:10.1016/j.quaint.2018.03.040

Li, B. F., Li, Q. F., Li, Y. F., Li, Z. J., Wang, F., Wang, X., et al. (2020a). Stable oxygen and carbon isotope record from a drill core from the Hetao Basin in the upper reaches of the Yellow River in northern China and its implications for paleolake evolution. *Chem. Geol.* 557, 119798. doi:10.1016/j.chemgeo.2020.119798

Li, G. Q., Zhang, H. X., Liu, X. J., Yang, H., Wang, X. Y., Zhang, X. J., et al. (2020b). Paleoclimatic changes and modulation of East Asian summer monsoon by high-latitude forcing over the last 130,000 years as revealed by independently dated loess-paleosol sequences on the NE Tibetan Plateau. *Quat. Sci. Rev.* 237, 106283. doi:10.1016/j.quascirev.2020.106283

Liu, Z. Q. (2020). *The optically stimulated luminescence chronology and environmental significance of palaeoflood in the Qaidam Basin*. [master's thesis]. China: Shandong Normal University.

Liu, Z. Q., Yu, L. P., An, P., Cao, M., Shen, H. Y., and Jiang, Y. J. (2019). Grain size characteristics of the Palaeoflood sediments in the middle stream of the Xiariha River in the Qaidam Basin. *Journal of Linyi University* 41, 76–86 (in Chinese). doi:10.13950/j.cnki.jlu.2019.06.0013

Lu, H. Y., Yi, S. W., Xu, Z. W., Zhou, Y. L., Zeng, L., Zhu, F. Y., et al. (2013). Chinese deserts and sand fields in last glacial maximum and Holocene optimum. *Chin. Sci. Bull.* 58 (23), 2775–2783. doi:10.1007/s11434-013-5919-7

Magaritz, M., and Enzel, Y. (1990). Standing-water deposits as indicators of Late Quaternary dune migration in the northwestern Negev, Israel. *Clim. Change* 16, 307–318. doi:10.1007/bf00144506

Murray, A. S., and Wintle, A. G. (2000). Luminescence dating of quartz using an improved single-aliquot regenerative-dose protocol. *Radia. Meas.* 32, 57–73. doi:10.1016/S1350-4487(99)00253-X

Murray, A. S., and Wintle, A. G. (2003). The single aliquot regenerative dose protocol: Potential for improvements in reliability. *Radia. Meas.* 37, 377–381. doi:10.1016/S1350-4487(03)00053-2

Nie, J. S., Stevens, T., Rittner, M., Stockli, D., Garzanti, E., Limonta, M., et al. (2015). Loess Plateau storage of northeastern Tibetan plateau-derived Yellow River sediment. *Nat. Commun.* 6, 8511. doi:10.1038/ncomms9511

Pan, B. T., Su, H., Hu, Z. B., Hu, X. F., Gao, H. S., Li, J. J., et al. (2009). Evaluating the role of climate and tectonics during non-steady incision of the Yellow River: Evidence from a 1.24Ma terrace record near Lanzhou, China. *Quat. Sci. Rev.* 28, 3281–3290. doi:10.1016/j.quascirev.2009.09.003

Pan, B. T., Hu, Z. B., Wang, J. P., Vandenberghe, J., and Hu, X. F. (2011). A magnetostratigraphic record of landscape development in the eastern Ordos Plateau, China: Transition from late miocene and early pliocene stacked sedimentation to late pliocene and quaternary uplift and incision by the Yellow River. *Geomorphology* 125, 225–238. doi:10.1016/j.geomorph.2010.09.019

Prescott, J. R., and Hutton, J. T. (1994). Cosmic ray contributions to dose rates for luminescence and ESR dating: Large-depths and long-term time variations. *Radia Meas.* 23, 497–500. doi:10.1016/1350-4487(94)90086-8

Roberts, H. M., and Duller, G. A. T. (2004). Standardised growth curves for optical dating of sediment using multiple-grain aliquots. *Radia. Meas.* 38, 241–252. doi:10.1016/j.radmeas.2003.10.001

Robins, L., Roskin, J., Yu, L. P., Bookman, R., and Greenbaum, N. (2022). Aeolian-fluvial processes control landscape evolution along dunefield margins of the northwestern Negev (Israel) since the late Quaternary. *Quat. Sci. Rev.* 285, 107520. doi:10.1016/j.quascirev.2022.107520

Roskin, J., Bookman, R., Friesem, D. E., and Vardi, J. (2017). A late Pleistocene linear dune dam record of aeolian-fluvial dynamics at the fringes of the northwestern Negev dunefield. *Sediment. Geol.* 353, 76–95. doi:10.1016/j.sedgeo.2017.03.011

Shen, J. (2012). Spatiotemporal variations of Chinese lakes and their driving mechanisms since the last glacial maximum: A review and synthesis of lacustrine sediment archives. *Chin. Sci. Bull.* 58, 17–31. (In Chinese). doi:10.1007/s11434-012-5510-7

Spratt, R. M., and Lisiecki, L. E. (2016). A late pleistocene Sea level stack. *Clim. Past* 12 (4), 1079–1092. doi:10.5194/cp-12-1079-2016

Sun, Y. B., Clemens, S. C., Guo, F., Liu, X., Wang, Y., Yan, Y., et al. (2021). High-sedimentation-rate loess records: A new window into understanding orbital- and millennial-scale monsoon variability. *Earth-Science Rev.* 220, 103731. doi:10.1016/j.earscirev.2021.103731

Thiel, C., Buylaert, J. P., Murray, A., Terhorst, B., Hofer, I., Tsukamoto, S., et al. (2011). Luminescence dating of the Stratzing loess profile (Austria) – testing the potential of an elevated temperature post-IR IRSL protocol. *Quatern. Int.* 234, 23–31. doi:10.1016/j.quaint.2010.05.018

Vermeersch, P. M., and Neer, W. V. (2015). Nile behaviour and late palaeolithic humans in upper Egypt during the late pleistocene. *Quat. Sci. Rev.* 130, 155–167. doi:10.1016/j.quascirev.2015.03.025

Wang, S. M., Xue, B., Shen, J., and Yao, S. C. (2009). The Lake environment changes in China and its mechanical explanation. *Geol. J. China Univ.* 15, 141–148. (In Chinese). doi:10.3969/j.issn.1006-7493.2009.02.001

Wang, Y. X., Chen, T. Y., E, C. Y., An, F. Y., Lai, Z. P., Zhao, L., et al. (2018). Quartz OSL and K-feldspar post-IR IRSL dating of loess in the Huangshui river valley, northeastern Tibetan plateau. *Aeolian Res.* 33, 23–32. doi:10.1016/j.aeolia.2018.04.002

Wei, G. X., Rao, Z. G., Dong, J., Yue, N., Dang, H. H., and Dong, Y. (2016). Late Quaternary climatic influences on megalake Jilantai–Hetao, North China, inferred from a water balance model. *Paleolimnol* 55, 223–240. doi:10.1007/s10933-015-9876-9

Wintle, A. G., and Murray, A. S. (2006). A review of quartz optically stimulated luminescence characteristics and their relevance in single-aliquot regeneration dating protocols. *Radia Meas.* 41, 369–391. doi:10.1016/j.radmeas.2005.11.001

Xie, F. B., Zhao, G. J., Mu, X. M., Gao, P., and Sun, W. Y. (2021). Variation of runoff and sediment load in the mainstream of the Yellow River over the past 70 years. *Sci. Soil Water Conservation* 19, 1–5. (In Chinese). doi:10.16843/j.sswc.2021.05.001

Xu, Z. W., Lu, H. Y., Yi, S. W., Vandenberghe, J., Mason, j., Zhou, Y., et al. (2015). Climate-driven changes to dune activity during the Last Glacial Maximum and deglaciation in the Mu Us dune field, north-central China. *Earth Planet Sci. Lett.* 427, 149–159. doi:10.1016/J.EPSL.2015.07.002

Yang, X. C., Cai, M. T., Ye, P. S., Yang, Y. B., Wu, Z. Q., Zhou, Q., et al. (2018). Late pleistocene paleolake evolution in the Hetao Basin, inner Mongolia, China. *Quatern. Int.* 464, 386–395. doi:10.1016/j.quaint.2017.11.047

Yang, X. C., Cai, M. T., Ye, P. S., Hu, J. M., Ji, F. B., Zhang, Z. G., et al. (2020). The paleolake hydrology and climate change since the ~40 ka in the Hetao Basin, Inner Mongolia, China. *Quatern. Int.* 553, 73–82. doi:10.1016/j.quaint.2020.06.040

Yang, X. Y., Yu, L. P., Chang, Q. F., and Lai, Z. P. (2022). Flood activity revealed millennial-scale climatic changes during the late Holocene in the Qaidam Basin, northeastern Tibetan Plateau. *Quatern. Int.* 637, 32–43. doi:10.1016/j.quaint.2022.06.011

Yu, L. P., Lai, Z. P., An, P., Pan, T., and Chang, Q. F. (2015). Aeolian sediments evolution controlled by fluvial processes, climate change and human activities since LGM in the Qaidam Basin, Qinghai-Tibetan Plateau. *Quatern. Int.* 372, 23–32. doi:10.1016/j.quaint.2014.09.043

Yu, L. P., Sun, Y., An, P., Greenbaum, N., and Roskin, J. (2022). Dunefield expansion and paleoclimate during MIS 3 in the Qaidam Basin, northeastern Tibetan plateau: Evidence from aeolian-fluvial processes and revised luminescence chronologies. *CATENA* 215, 106354. doi:10.1016/j.catena.2022.106354

Zhao, Q., An, P., Yu, L. P., and An, Q. (2016). Influence and significance of organic content on grain size of aeolian deposits. *J. Liaocheng Univ.* 04, 39–45. (In Chinese). doi:10.3969/j.issn.1672-6634.2016.04.009